Published in final edited form as:
Bone. 2012 January ; 50(1): 14–22. doi:10.1016/j.bone.2011.08.028.

Cortical Bone Resorption Following Muscle Paralysis is Spatially Heterogeneous

Brandon J. Ausk, **Philippe Huber**, **Sandra L. Poliachik**, **Steven D. Bain**, **Sundar Srinivasan**, and **Ted S. Gross**
Orthopaedics and Sports Medicine, University of Washington, Seattle, WA

Abstract

Mechanical loading of the skeleton, as induced by muscle function during activity, plays a critical role in maintaining bone homeostasis. It is not understood, however, whether diminished loading (and thus diminished mechanical stimuli) directly mediates the bone resorption that is associated with disuse. Our group has recently developed a murine model in which we have observed rapid and profound bone loss in the tibia following transient paralysis of the calf muscles. As cortical bone loss is achieved via rapid endocortical expansion without alterations in periosteal morphology, we believe this model holds unique potential to explore the spatial relation between altered mechanical stimuli and subsequent bone resorption. Given the available literature, we hypothesized that endocortical resorption following transient muscle paralysis would be spatially homogeneous. To test this hypothesis, we first validated an image registration algorithm that quantified site-specific cortical bone alterations with high precision and accuracy. We then quantified endocortical expansion in the tibial diaphysis within 21 days following transient muscle paralysis and found that, within the analyzed mid-diaphyseal region (3.15 mm), site-specific bone loss was focused on the anterior surface in the proximal region but shifted to the posterior surface at the distal end of the analyzed volume. This site-specific, but highly repeatable biologic response suggests active osteoclast chemotaxis or focal activation of osteoclastic resorption underlies the spatially consistent endocortical resorption induced by transient muscle paralysis. Clarifying this relation holds potential to yield unique insight into how the removal of factors critical for bone homeostasis acutely precipitates local modulation of cellular responses within bone.

Keywords

bone; bone resorption; focal bone loss; micro-CT; muscle paralysis; osteoclast

1.0 INTRODUCTION

Deficits in the skeleton's physiologic loading environment have potential to rapidly degrade bone mass and architecture presumably as a consequence of diminished mechanical stimuli [1–5]. Just as the anabolic response of bone to mechanical loading is focal and not systemic, the catabolic response of bone to disuse is also highly localized [6–9]. However, the biological processes mediating these highly localized bone alterations remain unclear.

Corresponding Author: Brandon Ausk, University of Washington, Department of Orthopaedics and Sports Medicine, Box 359798, 325 9th Ave, Seattle, WA 98104-2420, P: (206) 897-5610, F: (206) 897-5611, bjausk@u.washington.edu.

Previous investigations into the site-specificity of cortical bone resorption in models of bone loss are limited and have produced contrasting results. For example, in murine models of postmenopausal bone loss, highly heterogeneous alterations in cortical bone morphology were observed following OVX surgery [10, 11]. In contrast, complete functional deprivation via surgical osteotomies resulted in uniform bone resorption on the endocortical diaphyseal surface [12]. These findings suggest that the spatial pattern of bone loss may vary as a function of the stimulus for bone loss. If so, clarifying this spatial relation holds potential to yield unique insight into how the removal of factors critical for bone homeostasis acutely precipitates local modulation of cellular responses within bone.

In this context, the development of high-resolution micro-computed tomography (micro-CT) imaging systems capable of small animal *in vivo* scanning has enabled precise and accurate quantification of bone alterations in a variety of *in vivo* models [13, 14]. However, the ability to quantify site-specific bone alterations (e.g., a specific surface or portions of a surface within a volume of interest) across time requires the capability to accurately register serial *in vivo* images from the same bone. Initial attempts to identify locations of site-specific bone loss have used either mutual information strategies and/or relied upon user-defined landmarks for registration [10, 15]. However, the accuracy of such approaches will be compromised if the bone microarchitecture and associated landmarks used to register serial micro-CT volumes are themselves altered by the adaptive response. These challenges are amplified in models of trabecular bone adaptation, which demonstrate adaptive responses on all trabecular surfaces [5, 16, 17].

Alternatively, *in vivo* models of cortical bone adaptation have been observed to demonstrate surface specific adaptation in some experimental conditions. For example, we have reported that hindlimb muscle paralysis via injection of botulinum neurotoxin A (BTxA) induces profound acute cortical bone loss in the tibia [4, 5]. Morphologically, this loss of cortical bone emerges via acute osteoclast driven endocortical expansion, while the adjacent periosteal surface remains unchanged [4, 5, 18]. As such, we anticipated that this model would be amenable to serial *in vivo* image registration.

Based on the magnitude of acute bone resorption following transient muscle paralysis, which greatly exceeds disuse models that completely inhibit gait induced skeletal loading [19, 20], we hypothesized that cortical resorption following transient muscle paralysis would be spatially uniform around the endocortical surface. In order to test this hypothesis, we developed and validated an image registration paradigm that, when applied to our muscle paralysis model, accurately quantified site-specific cortical bone alterations without requiring user intervention. As this approach relied upon an assumption of a quiescent periosteal surface, we first assessed the precision and accuracy of our image registration method by quantifying the reproducibility of bone morphology parameters at increasing levels of detail in mice that were imaged twice, separated by 24 hours. Once validated, we then used this approach to quantify site-specific endocortical resorption following transient muscle paralysis.

2.0 METHODS

2.1 Transient Muscle Paralysis Model

All animal studies were performed in accordance with protocols approved by the Institutional Animal Care and Use Committee, University of Washington. Transient muscle paralysis was induced in the right calf muscle group of mice via a single injection of botulinum neurotoxin A (BTxA; 2U/100 g body weight) [4]. Mice received BTxA treatment on day 0 and were allowed free cage activity for the remainder of the experiment. This

intervention induces rapid and significant degradation of both trabecular and cortical bone compartments in the tibia [4, 5].

2.2 Experimental Design

Female C57Bl/6 mice were obtained from Jackson Laboratories with studies initiated when the mice reached 16 weeks of age. Three experiments were undertaken. The purpose of the first experiment was to validate the precision of the image registration approach. For this experiment, a group of untreated mice (Validation Group, n=6) were imaged on day 0 and again 24 hours later, a time interval in which no change in bone morphology could occur at the implemented imaging resolution. By eliminating potential morphology alterations, this analysis enabled volumetric registration of serial bone scans with only two sources of variability; that associated with the repeated positioning of the mice in the micro-CT scanner and the image acquisition variability native to the micro-CT scanner. The second experiment assessed our hypothesis that cortical resorption following transient muscle paralysis was spatially homogeneous. In this study, a group of mice did not receive BTxA and served as aged matched controls (Age-Matched Controls, n=6). A second group received BTxA injection in the right calf on day 0 (BTxA Group, n=14). Both groups were imaged on day 0 and again on day 21. The third and final experiment sought to establish an initial biological framework for the spatial pattern of osteoclastic resorption by comparing it to the patterns of osteoblastic activity at the endocortical surface. In this study, a group of untreated mice were injected with two Calcein labels (day 0 and day 9; 15 mg/kg i.p.) and standard dynamic histomorphometry was used to determine endocortical mineralizing surface (e.MS; Histomorphometry Group, n = 5).

2.3 Micro-CT Imaging

High-resolution micro-CT images of the right tibia midshaft were obtained for all mice on day 0 (Scanco CT 40; 10.5 μm voxel size, 55 kVp, 145 μA). While anesthetized with isoflurane, the right hindlimb of each mouse was secured in a custom apparatus in order to maximize the reproducibility of leg orientation and stability during the scan process. The imaged region spanned a 4.15 mm section of the tibia mid-diaphysis centered 2.75 mm proximal to the tibia-fibula junction (Fig 1A). A second scan of the same region was performed on the Validation Group 24 hours following the first imaging, and on day 21 for the Age-Matched Control and the BTxA Groups.

2.4 Image Registration

Prior to registration, all raw micro-CT image data was preprocessed using a Gaussian Filter algorithm to remove image noise (Sigma = 1.2, Support = 2.0), followed by cortical bone segmentation within the scan volume using standard image thresholding techniques [21]. Specifically, image data were binarized using a manufacturer recommended threshold for cortical bone identification (705.97 mg HA/cm^3) where dataset values greater than or equal to the threshold were considered calcified tissue.

Pilot studies examining cortical bone loss three weeks following calf paralysis indicated that the periosteal volume remained unchanged within the distal 50% of the scan volume (i.e., distal 2.1 mm) utilized in this study. We therefore used this region of the imaged bone as a registration landmark (i.e., registration volume) to register the entire secondary scan volume onto the primary scan volume obtained on day 0.

The endocortical volume of the binarized cortical bone volumes was digitally filled using custom image editing software (Matlab). The edited primary and secondary scans of individual mice (i.e., filled periosteal volumes) were registered using a vendor supplied 3-D image registration program (Scanco IPL Registration Command). Alignment of filled micro-

CT volumes was achieved through iterative identification of optimal translational and rotational parameters (Fig 1). Image registration was achieved via stepwise trial translations and rotations (using a combination of simplex and Powell's search methods) that minimized the function '*f*=1-r' (with 'r' being the correlation coefficient and 'r=1' representing a perfect correlation) [22, 23]. To avoid approaching 'local minima' solutions, image registration was performed initially on a courser resolution than the original scan volume (1/16 of original scan resolution). As the search neared a global minimum, the resolution increased to that of the original scan resolution in order to enable voxel accurate results. The procedure was iteratively performed until no further improvement in image registration was obtained (i.e., changes in '1-r' less than 1.0E-5). Thus, a secondary imaged volume of bone that was both translationally and rotationally out of alignment with the primary imaged volume was sequentially and progressively re-aligned with the primary imaged volume (Fig. 1). Once image rotational and translational parameters were identified that optimally registered the filled periosteal volumes, these parameters were then reapplied to the raw datasets (i.e., original scan datasets), allowing for image registration that did not rely on endocortical morphology.

2.5 Assessment of Cortical Bone Morphology

Following alignment, spatially-registered, raw serial micro-CT scans were exported to custom image processing software (in Matlab) for evaluation of bone morphology. The center 3.15 mm of each scan volume was used for analysis in all studies (the literature indicated that a ± 0.5 mm z-dimension variation in scan origins of serial micro-CT scans was sufficient to account for variability in z-dimension positioning of tibia; [24]). Cortical bone measures were quantified by summing the non-zero voxels in the thresholded binary data sets. To quantify periosteal measures, the endocortical volume within the cortical bone data sets was digitally filled using custom imaging software and non-zero voxels quantified. Endocortical measures were determined as the difference between periosteal and cortical datasets. Cortical porosities were treated as endocortical volume as it was assumed that they would be similarly affected by osteoclastic activity. As these porosities on average (± s.e.) account for only 0.6 ± 0.1% of the total endocortical volume, the total contribution of the cortical porosities to overall bone loss was minimal.

Cortical bone morphology was characterized at three levels of scale: 1) the entire analyzed scan volume (whole bone), 2) at seven transverse cross-sections equally spaced along the analyzed volume (cross-section), and 3) eight circumferential sectors within each of three cross-sections equally spaced along the analyzed volume (site-specific). The three equally spaced cross-sections examined in the site-specific analysis bracketed the analyzed volume and were labeled Proximal, Midshaft and Distal, respectively.

The morphologic parameters quantified at the whole bone level included periosteal volume (Ps.Vol), cortical volume (Ct.Vol) and endocortical volume (Ec.Vol). For cross-sectional and site-specific analyses, periosteal area (Ps.Ar), cortical area (Ct.Ar), and endocortical area (Ec.Ar) were quantified. To identify site-specific (i.e., circumferential) bone morphology, each primary and registered secondary 2-D cross-section was partitioned circumferentially into 8 equal angled sectors originating from the center of mass of the cortical bone cross-section of the primary (Day 0) scans. Eight sectors per cross-section were chosen based on pilot data indicating that further increasing sectors per cross-section did not improve the ability of this technique to identify focal circumferential bone changes (data not shown).

2.6 Outcome Measures

Bone morphology measures were determined at all three levels of scale and were used to assess the accuracy of the image registration approach (Validation Group) and the tissue location of cortical bone alterations (Age-Matched and BTxA Groups). Differences were determined by comparing the primary and registered secondary scans. Whole bone analysis quantified the percent difference of entire scan volumes. Cross-sectional analysis was used to assess bone alterations along the long-axis of the scan volume at each of seven equally spaced 2-D transverse cross-sections. Finally, site-specific circumferential bone morphology alterations within the Proximal, Midshaft and Distal cross-sections were quantified on a per sector basis.

2.6.1 Image Registration Accuracy—To quantify image registration accuracy, secondary (Day 1) scans were superimposed on primary (Day 0) scans for the Validation Group. The mean absolute percent error (MAPE) between the bone volume measures in the primary and registered secondary scan volumes were then calculated at the whole bone, cross-section and site-specific levels (i.e., perfectly aligned, volumetrically-identical serial scans would produce mean absolute percent errors of 0% for all measures at all scales).

To determine at which level of scale image registration became necessary to accurately reproduce morphologic measures, the MAPE calculated for registered secondary volumes was compared to the MAPE calculated for unregistered secondary volumes. To accomplish this, unregistered secondary images were assumed to have identical global coordinates as the primary images (e.g., the most distal cross-section in the unregistered secondary image corresponded with the most distal cross-section in the primary image).

Finally, we assessed the accuracy of the image registration technique (which relied on the assumption of a quiescent periosteal volume) in the presence of simulated endocortical bone resorption (i.e., mimicking the anticipated effect of BTxA). For this simulation, we digitally imposed homogeneous endocortical resorption onto the Day 1 scans. Specifically, a 31.5 micron thick volume of cortical bone was digitally removed homogeneously from the entire endocortical surface (altered Day 1 scans). Day 1 scans before and after simulated endocortical bone removal were identically oriented. Comparison of the altered and unaltered Day 1 scans did not require image registration and site-specific bone loss identified in this comparison therefore serve as the benchmark pattern of bone loss. We then registered altered Day 1 scans onto the Day 0 scans as described above, calculated site-specific endocortical bone loss at the Midshaft cross-section, and contrasted those data with the benchmark pattern of bone loss. This comparison enabled us to assess the accuracy of the image registration approach in the presence of significant, albeit digitally imposed, homogeneous endocortical expansion.

2.6.2 Bone Loss Induced by Muscle Paralysis—Changes in bone morphology induced by transient muscle paralysis were determined by assessing alterations in bone morphology (expressed as percent difference from Day 0) at each of the three levels of scale for Age-Matched Control and BTxA treated mice. A comparison of periosteal volumes was first performed to confirm that no significant alterations of the periosteal volume occurred within 21 days of BTxA treatment. Given our hypothesis and previous data demonstrating that cortical bone loss arises due to endocortical expansion, the site-specific analysis was confined to assessing alterations in endocortical area (Ec.Ar) at three equally spaced cross-sections along the scan volume.

2.6.3 Comparison of Endocortical Bone Formation and Bone Resorption—Endocortical mineralizing surface (e.MS) was quantified in the right tibia of

Histomorphometry mice using standard dynamic histomorphometry [25, 26]. To assess focal osteoblast function, e.MS was calculated within each of eight sectors (identical to the sector morphology analysis above) for both the Proximal and Distal cross-sections. Circumferential e.MS in the Histomorphometry mice (which were untreated) was then contrasted with locations of endocortical expansion induced in mice following transient muscle paralysis. To facilitate comparison of focally induced osteoclast activity vs baseline osteoblast activity, the endocortical expansion (BTxA Group) and e.MS (Histomorphometry Group) datasets were normalized by quantifying the contribution of each sector to the overall cross-section total (either total endocortical expansion or total e.MS).

2.7 Statistics

Paired T-tests were used to compare precision of the image registration algorithm to reproduce bone morphologic measures at all three scales investigated. Treatment effects of BTxA were determined by comparing differences in Age-Matched Control versus BTxA Groups using unpaired T-tests (at the whole bone level) and MANOVA with a Bonferroni post-hoc analysis (at the cross-section level). One-way ANOVA with a Bonferroni post-hoc analysis were used to determine circumferential non-uniformity of bone loss at the three individual cross-sections examined. The circumferential difference between e.MS in the Proximal and Distal cross-sections in untreated Histomorphometry mice were determined using unpaired T-tests. A focused ANOVA with a Bonferroni post-hoc analysis comparing sector differences in normalized e.MS and normalized endocortical expansion was used to contrast areas of baseline osteoblastic activity with focal areas of endocortical resorption induced by transient muscle paralysis. Statistical significance was determined at $p<0.05$ in all assessments.

3.0 RESULTS

3.1 Image Registration Accuracy

Using the periosteal volume as the registration landmark, our image registration approach produced highly correlated registered images in the Validation Group ($r=0.995 \pm 0.001$) requiring an average (± s.e.) of 282 ± 18 iterations per specimen to reach optimal registration parameter values. At the whole bone level, the MAPEs in both registered and unregistered scans were less than 0.5% regardless of morphologic outcome measure (Table 1). Similarly, the MAPEs for all morphology parameters in the transverse cross-section analysis were small (less than 1.0%) and not significantly different between registered and unregistered scans (Table 1). Image registration substantially improved the reproducibility with which bone morphology parameters could be measured at specific sites within a given cross-section. On a per sector basis, the MAPEs in registered scans were significantly reduced compared to unregistered scans for Ps.Ar ($p<0.02$), Ct.Ar ($p<0.03$) and Ec.Ar ($p<0.02$; Table 1).

Image registration did not affect the ability to accurately quantify a known simulated endocortical bone loss in the digitally altered Day 1 scans at any of the three levels of scale. At the whole bone level, there was no significant difference in the percent Ec.Vol alterations quantified in the benchmark and registered Day 1 scans (26.3 ± 0.4% vs 26.2 ± 0.5%, $p=0.73$). Similarly, endocortical expansions quantified at the cross-sectional level was similar in benchmark and registered Day 1 scans (26.4 ± 0.4% vs 26.3 ± 0.4%, $p=0.77$). Finally, a comparison of site-specific endocortical expansion at the Midshaft cross-section showed no significant difference between the quantified per sector bone loss in the benchmark and registered Day 1 scans for any sector (Fig. 2).

3.2 Cortical Bone Loss Induced by Transient Muscle Paralysis

At the whole bone level, muscle paralysis did not alter Ps.Vol compared to Age-Matched Control mice (−0.7 ± 0.3% versus −0.6 ± 0.3 %, respectively; $p>0.78$). As expected, muscle paralysis significantly decreased Ct.Vol over 3 weeks compared with Age-Matched Controls (−6.9 ± 1.1% versus 1.6 ± 0.9%, respectively; $p<0.001$), due to a significant expansion of Ec.Vol (9.4 ± 1.6% vs. −3.5 ± 1.7%, $p<0.001$).

At the cross-sectional level, changes in periosteal volume were small and non-significant in BTxA treated mice (ranging from 0.4% to −1.4%) and did not differ from Age-Matched Controls at any cross-section examined (Fig. 3). Within the distal region used to register the bone, where the assumption of unchanged periosteal volume was made, alterations in Ps.Ar were particularly small (between 0.4% to −0.5%). Muscle paralysis decreased Ct.Ar compared with Age-Matched Controls, with six of seven cross-sections demonstrating statistical significance (Fig. 3). Identical to the bone loss pattern identified at the whole bone level, decreased Ct.Ar arose via a significant increase in Ec.Ar in the BTxA treated group compared to Age-Matched Controls in all seven cross-sections (Fig. 3).

At the site-specific level, observed patterns of bone loss were in sharp contrast to our hypothesis that transient paralysis would induce uniform endocortical resorption. Specifically, the assessment of endocortical expansion in the three analyzed cross-sections spanning the mid-diaphysis region of interest revealed heterogeneous, but reproducible, patterns of bone resorption. At the Proximal location, mean endocortical expansion due to muscle paralysis was most heterogeneous (range: 36.4 to −3.9%) and focused primarily in the anterior sectors of the cross-section (Fig. 4). At the Midshaft, endocortical expansion was the most uniform, but still demonstrated regions of profound and minimal bone loss (19.9 to 5.2%; Fig. 4). Endocortical resorption in the Distal cross-section was also site-specific (28.1 to 4.9%, Fig. 4), but, in contrast with the Proximal cross-section, maximal bone resorption was focused within the posterior aspect of the cross-section.

3.3 Comparison of Endocortical Bone Formation and Bone Resorption

The spatial distribution of osteoblast activity varied between the Proximal and Distal cross-sections in untreated Histomorphometry mice (Table 2). For the Proximal cross-section, e.MS was significantly greater on the posterior/medial cortex (Sector 6, $p<0.05$), while at the Distal cross-section e.MS was significantly greater on the anterior/medial cortex (Sector 4, $p<0.02$; Table 2). Qualitatively, the sites of baseline endocortical osteoblast activity did not spatially correspond with sites of focal osteoclast activity (Fig. 5A&B). At the Proximal cross-section, the normalized baseline e.MS was significantly different from the normalized endocortical expansion induced in sector 6 ($p<0.03$, Fig. 5C). At the Distal cross-section, baseline normalized e.MS was significantly different from sites of induced osteoclast activity in sectors 3, 4, 6 and 7 ($p>0.04$, Fig. 5C).

4.0 DISCUSSION

Contrary to our hypothesis, we found that endocortical expansion induced by transient muscle paralysis of the calf was remarkably site-specific within the tibia mid-diaphysis of all mice. We identified this spatial pattern of bone resorption by developing and validating an automated image registration procedure that was capable of defining focal *in vivo* bone loss if the periosteal volume was unchanged during the experimental intervention. The reproducibility of sites of focal endocortical expansion across animals suggests a locally mediated process in which specific regions of the endocortical surface actively enhanced or inhibited osteoclastic attachment and/or resorption.

The literature describing site-specific bone loss has primarily focused upon the varied sensitivity of different skeletal regions to disuse [6, 27–29]. A single previous study reported uniform diaphyseal endocortical expansion following functional isolation of the turkey radius, though activation of intracortical resorption in this model was distinctly non-uniform [12]. Though these previous results, in part, led to our hypothesis, two differences between that study and the present study are likely to underlie the distinct results. First, the previous study used a best-fit strategy to align cross-sectional images that is likely to have biased assessment of focal endocortical resorption. Second, from a mechanical perspective, complete isolation from functional loading via osteotomies is likely to induce a much more profound deprivation of mechanical stimuli than transient calf paralysis.

We first determined the scale (whole bone, cross-section, or site-specific) at which our image registration approach was required to accurately identify biological adaptation given the variability inherent with repeatedly imaging the same region of cortical bone. This variability arises from a combination of the actual image acquisition by the micro-CT scanner and the reproducibility of aligning the specimen within the micro-CT scanner. We found that image registration produced no significant improvement in the ability to detect alterations that occur across or along the entire scan volume (i.e., no improvement on whole bone or transverse cross-section comparisons in Validation Group mice). This finding is consistent with recent published data showing that whole bone metric parameters are reproducible across scans [30]. However, image registration did significantly improve the ability to align bones circumferentially (as represented at the site-specific level). These results demonstrate that accurate *ex post facto* image registration is required in order for *in vivo* quantifications of site-specific bone alterations. Critically, it is this level of detail that is needed to explore focal cellular activity that is responsible for achieving acute bone adaptation.

In this study, we used the periosteal volume of the tibia mid-shaft as an unchanged landmark capable of registering serial images. This assumption requires that the periosteal volume (i.e., the filled volume) remains quiescent through the study duration (i.e., unchanged volume not a result of an equilibrium between bone resorption and apposition). We have previously published dynamic histomorphometric data indicating that osteoblast activity on the periosteal surface of the tibia mid-diaphysis was not altered when the calf is paralyzed by BTxA [5]. These data, taken with unchanged micro-CT periosteal volume measures identified both in this study and in previous studies [5], confirms that the tibia mid-shaft periosteal volume remained quiescent for up to 3 weeks following transient calf muscle paralysis.

Identification of an invariant registration landmark within *in vivo* models that also demonstrate profound alterations in bone morphology has been a primary impediment to using serial high-resolution micro-CT imaging to accurately quantify site-specific bone adaptation. To circumvent this problem, previous studies have used operator-defined regions of interest (ROI) to enable alignment of micro-CT images across time via mutual information registration [10, 15]. The implicit assumption is that the bone morphology within the user identified ROI is unvarying through the experiment or that bone apposition/resorption is uniform on all surfaces. Our image registration methodology differs in that we defined the absence of periosteal adaptation through the mid-diaphysis and thus avoided manual identification of registration landmarks or the assumption of uniform bone apposition/resorption. Given the unchanged periosteal volume, we were then able to assess the accuracy of our image registration approach in animals with substantial cortical bone loss. This advancement has allowed us to use serial micro-CT images to quantify the morphologic result of osteoclast activity, while previous image registration techniques were limited to use for qualitative assessment of bone alterations [15]. As the novelty of our

approach lies with the application of the image registration algorithm (rather than its development), the accuracy and precision of superpositioning unaltered whole bone volumes in our study is similar to those described in other image registration studies [10, 30]. We also assessed our ability to accurately quantify endocortical bone alterations by digitally manipulating the endocortical surface in the Validation Group's Day 1 scans. By comparing this known bone loss (i.e., benchmark bone loss pattern) to that quantified when the altered Day 1 scans were registered on the Day 0 scans, we demonstrated that the image registration approach itself did not affect our ability to accurately quantify focal endocortical bone resorption.

Conceptually, our image registration methodology could be implemented in any animal model in which one cortical surface remains constant through the experiment (i.e., resulting in a constant endocortical or periosteal scan volume). Thus, under anabolic conditions, the strategy could be extended to quantify periosteal adaption should the endocortical surface remain unchanged [26, 31]. However, a clear limitation of our approach is the inability to serially register micro-CT images of bone regions in which both surfaces are modified during the experiment. Given this limitation, our registration strategy would be best implemented in models that demonstrate rapid, surface-specific bone resorption or formation, as longer time course experiments in rodents will inevitably be confounded by surface modeling [32, 33].

While it is not possible to directly apply our current approach to explore *in vivo* alterations in trabecular morphology (in the absence of a quiescent surface our approach regresses to a best-fit algorithm), it is conceptually possible to extend the strategy to study focal trabecular adaptation. The primary challenge is that acute trabecular adaptation to mechanical loading, disuse, or alterations in systemic hormones is not confined to a single surface [6, 11, 34]. One possible solution would be to simply use our present registration technique on an expanded scan volume that encompassed the entire bone length in order to identify an unchanged surface. However, such an extended scan volume would greatly increase radiation exposure and time under anesthesia, both of which may be deleterious for normal skeletal health in mice [35]. Instead, we anticipate that accurate trabecular registration could be accomplished by scanning two distinct but smaller volumes (e.g., an unchanged registration volume within the mid-diaphysis and a spatially non-contiguous region spanning the epiphysis and metaphysis). Translational and rotational parameters for the accurate superpositioning for the mid-diaphysis could be applied to the region of interest by using global micro-CT image coordinates that reference the relative position of non-contiguous bone scans obtained within a single scanning session. This extension would allow for mapping of bone alterations at any skeletal location as long as an unchanged bone volume (periosteal or endocortical) was available within the same micro-CT scanning session and was part of the same bone 'rigid-body.' Ongoing preliminary studies support further investigation of this strategy [36].

In the current study, we were able to generate a 3-D map of endocortical bone resorption at the tibia mid-shaft following transient paralysis of the calf muscles. In contrast with our hypothesis, regions of focal endocortical resorption were clearly activated along the long axis of the tibia, even within the relatively small analyzed portion of the mid-diaphysis (20% of total diaphyseal length). The consistency of the asymmetric spatial pattern of bone resorption following muscle paralysis suggests that osteoclasts were not homogeneously distributed along the endocortical bone surface, but rather directly recruited to specific surface locations. Resorption in the proximal analysis region was focused on the anterior endocortical surface but resorption in the distal analyzed region was focused on the posterior endocortical surface. As the calf muscle group spans the entire diaphyseal region of study,

this result implied that direct spatial association with the paralyzed muscle is not likely to be the primary mediator of acute focal bone resorption in this model.

Alternatively, given the relation between mechanical stimuli and bone morphology [37–39], it might be suggested that the regions of focal resorption correspond with regions of maximally decreased bone strain. As the gait defect induced by calf paralysis is mild and transient [5], it would be reasonable to assume that the regions of peak tension and compression during gait would be the sites of greatest change in locomotion-induced strain. However, we have recently quantified peak normal strains in the mouse tibia during locomotion, and neither the location of peak tension (anterior/lateral cortex) or peak compression (posterior/medial cortex) corresponds with the regions of focal bone resorption [40].

Given the apparent lack of relation between maximal endocortical resorption and diminished mechanical stimuli, we attempted to determine if normal endocortical osteoblastic was spatially associated with focal activation of resorption in the model (or the lack of resorption). We found that regions with significant osteoblastic activity (as defined by Calcein labeling) were spatially associated with minimal osteoclastic resorption following muscle paralysis. While preliminary, these data suggest that muscle paralysis induced endocortical resorption was minimally initiated in regions normally undergoing endocortical modeling. Instead, endocortical expansion appeared focused upon surfaces quiescent in naïve mice (or, potentially, accelerated at sites already undergoing modeling associated resorption). These data are consistent with an accentuation of the resorptive aspect of normal cortical bone modeling drift in which accumulated endocortical resorption tends to proceed on the opposite part of the cross-section from accumulated bone formation [41]. A clear limitation of these observations is that quantification of focal endocortical osteoblast and osteoclast activity where performed on separate groups of mice. However, if these preliminary data were substantiated with more extensive histomorphometry, it would suggest that specific cortical regions are more predisposed to acute bone resorption following muscle paralysis. As such, this type of focal loss could disproportionately diminish bone strength, depending on the plane of bending of the bone.

In summary, we quantified focal areas of acute endocortical resorption within the tibia mid-diaphysis following transient calf paralysis via a single injection of BTxA. To accomplish this goal, we developed and validated a novel approach capable of automated quantification of spatial osteoclastic activity in a model of acute bone resorption. Surprisingly, we found that even within a small volume of the diaphysis, maximal endocortical resorption consistently shifted from the anterior to posterior surface while moving proximally to distally through a relatively small volume of interest. Given the consistent spatial recruitment of osteoclasts following muscle paralysis, we anticipate that future studies hold the potential to clarify the cellular signaling underlying this locally mediated process and thereby identify new strategies for intervening in a variety of bone loss pathologies.

Highlights

We validated an imaging approach to quantify endocortical bone resorption *in vivo*.

We found that endocortical resorption induced by muscle paralysis was site-specific.

This response was consistent with local modulation of osteoclast function.

Acknowledgments

This work was supported in part by a F31 Fellowship from the NIA (F31AG037287), NIAMS (AR 45665, AR60304) and the Sigvard T. Hansen, Jr. Endowed Chair. The authors also thank Andres Laib, Ph.D., for his assistance in installing the necessary algorithm code.

REFERENCES

1. Bloomfield SA, Allen MR, Hogan HA, Delp MD. Site- and compartment-specific changes in bone with hindlimb unloading in mature adult rats. Bone. 2002; 31(1):149–157. [PubMed: 12110428]
2. Damrongrungruang T, Kuroda S, Kondo H, Aoki K, Ohya K, Kasugai S. A simple murine model for immobilization osteopenia. Clin Orthop Relat Res. 2004; (425):244–251. [PubMed: 15292815]
3. Gross TS, Damji AA, Judex S, Bray RC, Zernicke RF. Bone hyperemia precedes disuse-induced intracortical bone resorption. J Appl Physiol. 1999; 86(1):230–235. [PubMed: 9887135]
4. Poliachik SL, Bain SD, Threet D, Huber P, Gross TS. Transient muscle paralysis disrupts bone homeostasis by rapid degradation of bone morphology. Bone. 2010; 46(1):18–23. [PubMed: 19857614]
5. Warner SE, Sanford DA, Becker BA, Bain SD, Srinivasan S, Gross TS. Botox induced muscle paralysis rapidly degrades bone. Bone. 2006; 38(2):257–264. [PubMed: 16185943]
6. Judex S, Garman R, Squire M, Busa B, Donahue LR, Rubin C. Genetically linked site-specificity of disuse osteoporosis. J Bone Miner Res. 2004; 19(4):607–613. [PubMed: 15005848]
7. Marenzana M, De Souza RL, Chenu C. Blockade of beta-adrenergic signaling does not influence the bone mechano-adaptive response in mice. Bone. 2007; 41(2):206–215. [PubMed: 17543595]
8. Robling AG, Niziolek PJ, Baldridge LA, Condon KW, Allen MR, Alam I, Mantila SM, Gluhak-Heinrich J, Bellido TM, Harris SE, Turner CH. Mechanical stimulation of bone in vivo reduces osteocyte expression of Sost/sclerostin. J Biol Chem. 2008; 283(9):5866–5875. [PubMed: 18089564]
9. Sugiyama T, Price JS, Lanyon LE. Functional adaptation to mechanical loading in both cortical and cancellous bone is controlled locally and is confined to the loaded bones. Bone. 46(2):314–321. [PubMed: 19733269]
10. Waarsing JH, Day JS, van der Linden JC, Ederveen AG, Spanjers C, De Clerck N, Sasov A, Verhaar JA, Weinans H. Detecting and tracking local changes in the tibiae of individual rats: a novel method to analyse longitudinal in vivo micro-CT data. Bone. 2004; 34(1):163–169. [PubMed: 14751574]
11. Waarsing JH, Day JS, Verhaar JA, Ederveen AG, Weinans H. Bone loss dynamics result in trabecular alignment in aging and ovariectomized rats. J Orthop Res. 2006; 24(5):926–935. [PubMed: 16583450]
12. Gross TS, Rubin CT. Uniformity of resorptive bone loss induced by disuse. J Orthop Res. 1995; 13(5):708–714. [PubMed: 7472749]
13. Rüegsegger P, Koller B, Müller R. A microtomographic system for the nondestructive evaluation of bone architecture. Calcif Tissue Int. 1996; 58(1):24–29. [PubMed: 8825235]
14. Stenstrom M, Olander B, Carlsson CA, Carlsson GA, Lehto-Axtelius D, Hakanson R. The use of computed microtomography to monitor morphological changes in small animals. Appl Radiat Isot. 1998; 49(5–6):565–570. [PubMed: 9569543]
15. Boyd SK, Moser S, Kuhn M, Klinck RJ, Krauze PL, Müller R, Gasser JA. Evaluation of three-dimensional image registration methodologies for in vivo micro-computed tomography. Ann Biomed Eng. 2006; 34(10):1587–1599. [PubMed: 16957987]
16. Brouwers JE, Lambers FM, van Rietbergen B, Ito K, Huiskes R. Comparison of bone loss induced by ovariectomy and neurectomy in rats analyzed by in vivo micro-CT. J Orthop Res. 2009; 27(11): 1521–1527. [PubMed: 19437511]
17. David V, Laroche N, Boudignon B, Lafage-Proust MH, Alexandre C, Ruegsegger P, Vico L. Noninvasive in vivo monitoring of bone architecture alterations in hindlimb-unloaded female rats using novel three-dimensional microcomputed tomography. J Bone Miner Res. 2003; 18(9):1622–1631. [PubMed: 12968671]

18. Warner SE, Srinivasan S, Kostenuik PJ, Gross TS. RANKL inhibition prevents the loss of bone volume and bone strength caused by Botox induced muscle paralysis. 52nd Trans Orthop Res Soc. 2006; 31:189.
19. Morey-Holton ER, Globus RK. Hindlimb unloading rodent model: technical aspects. J Appl Physiol. 2002; 92(4):1367–1377. [PubMed: 11895999]
20. Gross TS, Poliachik SL, Prasad J, Bain SD. The effect of muscle dysfunction on bone mass and morphology. J Musculoskelet Neuronal Interact. 2010; 10(1):25–34. [PubMed: 20190377]
21. Stauber M, Muller R. Micro-computed tomography: a method for the non-destructive evaluation of the three-dimensional structure of biological specimens. Methods Mol Biol. 2008; 455:273–292. [PubMed: 18463825]
22. Sutton MA, Cheng MQ, Peters WH, Chao YJ, Mcneill SR. Application of an Optimized Digital Correlation Method to Planar Deformation Analysis. Image and Vision Computing. 1986; 4(3): 143–150.
23. Verhulp E, van Rietbergen B, Huiskes R. A three-dimensional digital image correlation technique for strain measurements in microstructures. Journal of Biomechanics. 2004; 37(9):1313–1320. [PubMed: 15275838]
24. Boutroy S, Bouxsein ML, Munoz F, Delmas PD. In vivo assessment of trabecular bone microarchitecture by high-resolution peripheral quantitative computed tomography. J Clin Endocrinol Metab. 2005; 90(12):6508–6515. [PubMed: 16189253]
25. Srinivasan S, Agans SC, King KA, Moy NY, Poliachik SL, Gross TS. Enabling bone formation in the aged skeleton via rest-inserted mechanical loading. Bone. 2003; 33(6):946–955. [PubMed: 14678854]
26. Srinivasan S, Ausk BJ, Poliachik SL, Warner SE, Richardson TS, Gross TS. Rest-inserted loading rapidly amplifies the response of bone to small increases in strain and load cycles. J Appl Physiol. 2007; 102(5):1945–1952. [PubMed: 17255366]
27. Lang T, LeBlanc A, Evans H, Lu Y, Genant H, Yu A. Cortical and trabecular bone mineral loss from the spine and hip in long-duration spaceflight. J Bone Miner Res. 2004; 19(6):1006–1012. [PubMed: 15125798]
28. Bain SD, Rubin CT. Metabolic modulation of disuse osteopenia: endocrine-dependent site specificity of bone remodeling. J Bone Miner Res. 1990; 5(10):1069–1075. [PubMed: 2080718]
29. Vico L, Collet P, Guignandon A, Lafage-Proust MH, Thomas T, Rehaillia M, Alexandre C. Effects of long-term microgravity exposure on cancellous and cortical weight-bearing bones of cosmonauts. Lancet. 2000; 355(9215):1607–1611. [PubMed: 10821365]
30. Nishiyama KK, Campbell GM, Klinck RJ, Boyd SK. Reproducibility of bone micro-architecture measurements in rodents by in vivo micro-computed tomography is maximized with three-dimensional image registration. Bone. 2010; 46(1):155–161. [PubMed: 19796719]
31. Moustafa A, Sugiyama T, Saxon LK, Zaman G, Sunters A, Armstrong VJ, Javaheri B, Lanyon LE, Price JS. The mouse fibula as a suitable bone for the study of functional adaptation to mechanical loading. Bone. 2009; 44(5):930–935. [PubMed: 19442626]
32. Jee, WSS. The skeletal tissues, in Cell and Tissue Biology: A Textbook of Histology. Weiss, L., editor. Baltimore: Urban and Schwartzenberg; 1989. p. 211-259.
33. Frost, HM. The Henry Ford Hospital surgical monographs. Vol. xiii. C.C. Thomas: Springfield, Ill; 1964. The laws of bone structure; p. 167
34. Lee KC, Maxwell A, Lanyon LE. Validation of a technique for studying functional adaptation of the mouse ulna in response to mechanical loading. Bone. 2002; 31(3):407–412. [PubMed: 12231414]
35. Klinck RJ, Campbell GM, Boyd SK. Radiation effects on bone architecture in mice and rats resulting from in vivo micro-computed tomography scanning. Med Eng Phys. 2008; 30(7):888–895. [PubMed: 18249025]
36. Ausk, BJ.; Huber, P.; Srinivasan, S.; Bain, SD.; Gross, TS. Initiation of trabecular bone resorption following transient muscle paralysis is site specific. 2011 Orthopaedic Research Society Annual Meeting; Long Beach, CA. 2011. Abstract #2260
37. Chamay A, Tschantz P. Mechanical influences in bone remodeling. Experimental research on Wolff's law. J Biomech. 1972; 5(2):173–180. [PubMed: 5020948]

38. Goodship AE, Lanyon LE, McFie H. Functional adaptation of bone to increased stress. An experimental study. J Bone Joint Surg Am. 1979; 61(4):539–546. [PubMed: 438241]

39. Frost HM. Bone "mass" and the "mechanostat": a proposal. Anat Rec. 1987; 219(1):1–9. [PubMed: 3688455]

40. Prasad J, Wiater BP, Nork SE, Bain SD, Gross TS. Characterizing gait induced normal strains in a murine tibia cortical bone defect model. J Biomech. 2010; 43(14):2765–2770. [PubMed: 20674920]

41. Frost HM. Mechanical determinants of bone modeling. Metab Bone Dis Relat Res. 1982; 4(4): 217–229. [PubMed: 6763662]

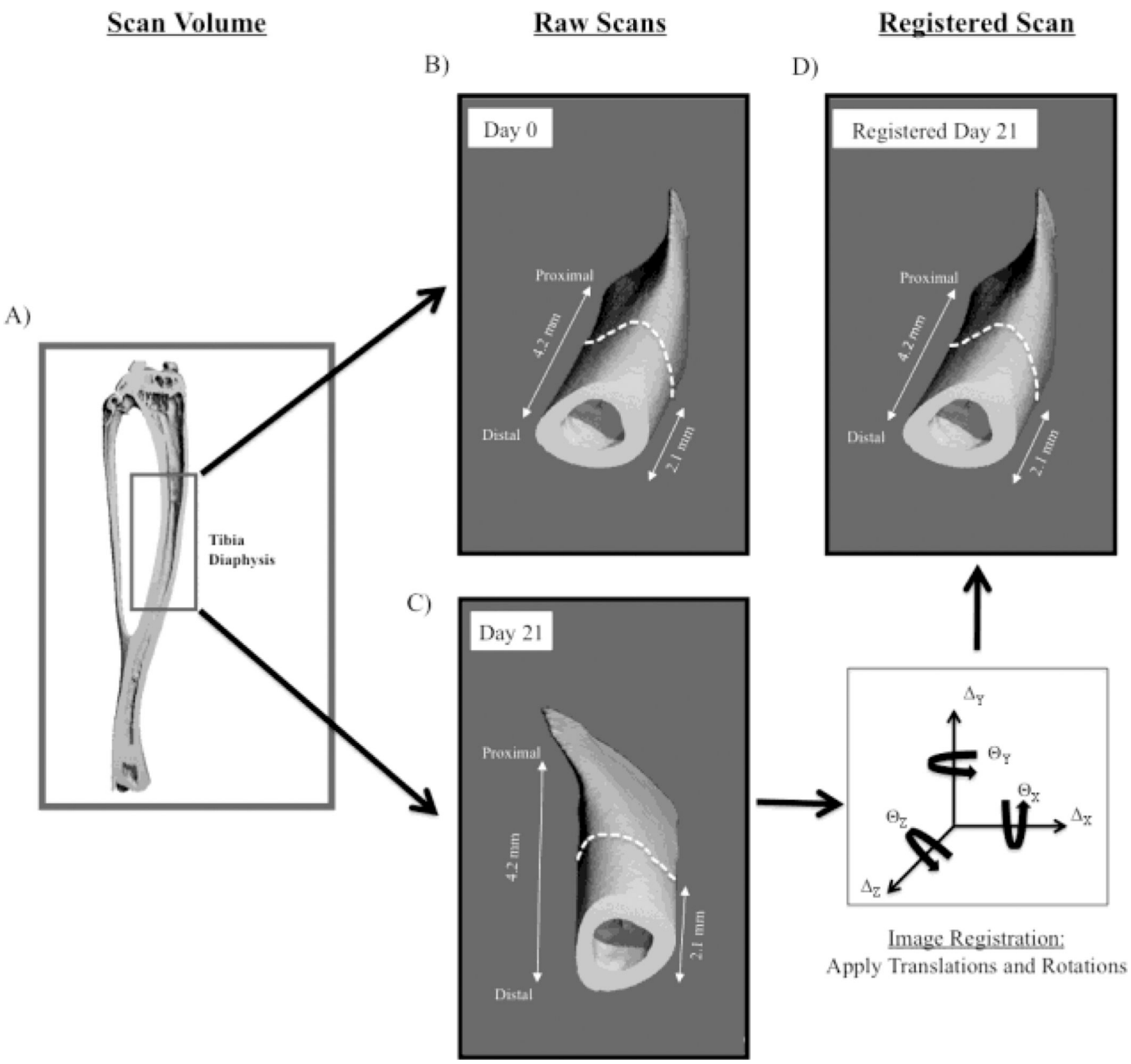

Fig. 1.

Serial micro-CT scans of 4.15 mm of the tibia diaphysis (A, inset box) were obtained prior to BTxA injection (B, Day 0) with a secondary scan obtained 3 weeks later (C, or 1 day later in Validation Group). The secondary scan was then registered onto the primary scan (D) using the periosteal volume of the distal 2.1 mm of the imaged region as the registration landmark.

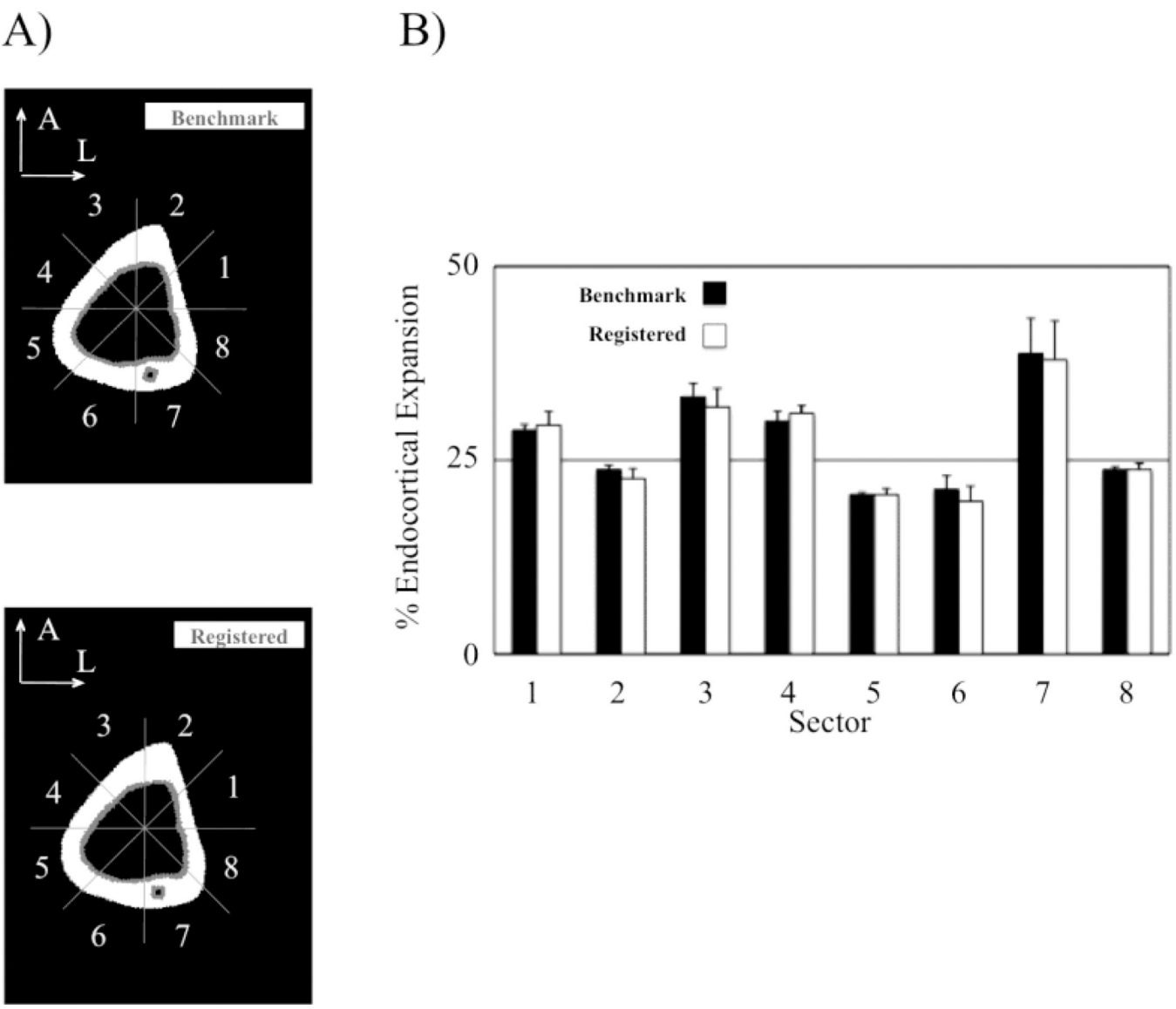

Fig. 2.

To measure the ability of our image registration approach to accurately quantify a known bone loss pattern, homogeneous endocortical resorption was digitally applied to each Day 1 scan volume in the Validation Group (−17.9 ± 0.2% induced cortical bone loss). Comparing the digitally altered Day 1 scans to the unaltered Day 1 scans allowed for quantification of a known bone loss pattern (Benchmark; A). The benchmark was than compared to the bone loss pattern observed when the altered Day 1 scans were registered onto the Day 0 scans (Registered, with resorption in gray). No significant differences were identified in the circumferential bone loss calculated at any sector (B; $p>0.95$).

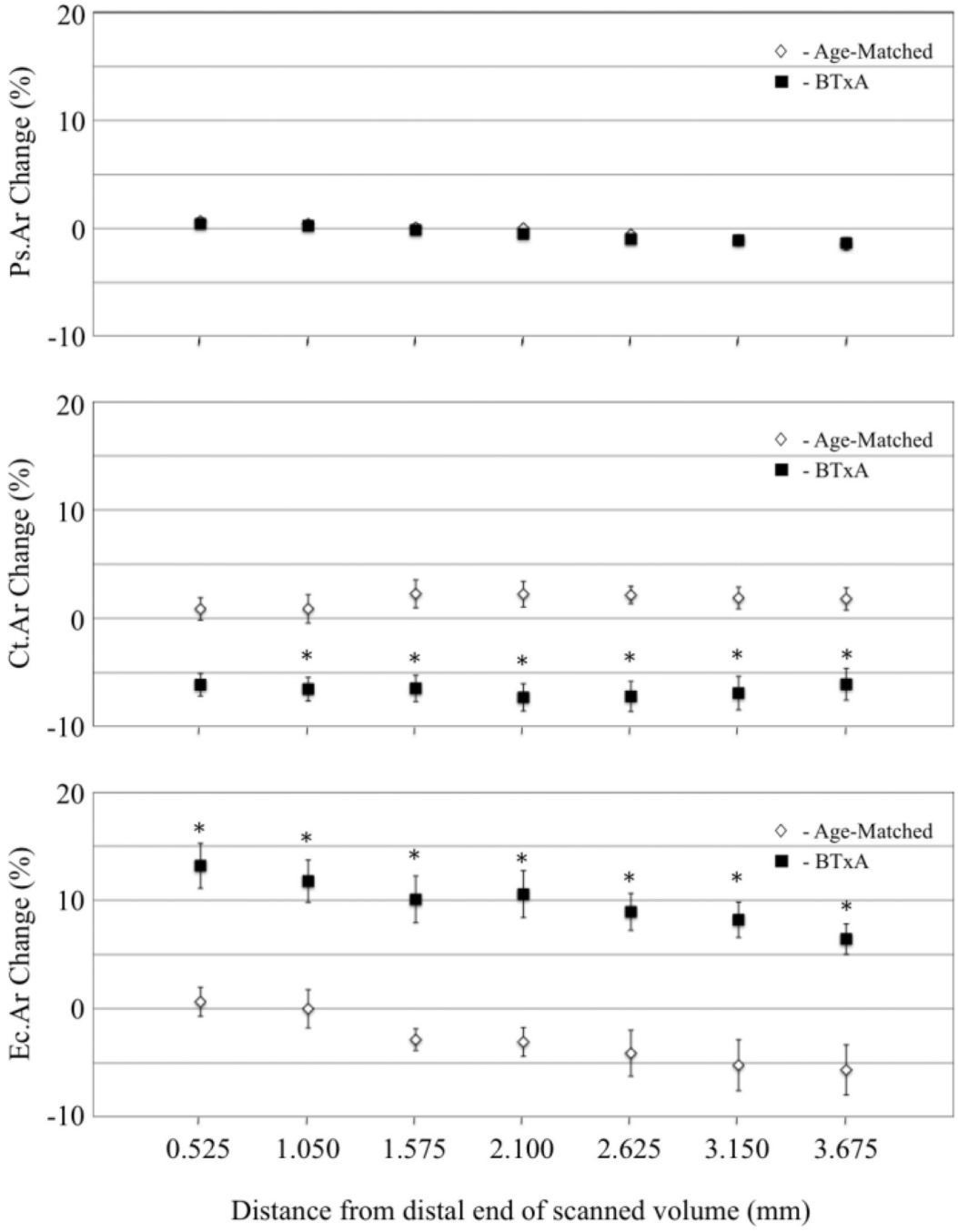

Fig. 3.

Transient muscle paralysis did not alter periosteal surface changes (A; Ps.Ar) at the analyzed 2-D transverse cross-sections in Age-Matched (white diamond, partially obscured b overlying BTxA data) vs BTxA mice (black square, mean ± s.e.). In contrast, significant differences in cortical (Ct.Ar) and endocortical morphology (Ec.Ar) were identified at all but one cross-section examined in BTxA vs Age-Matched Control mice (*, significantly differences vs. BTxA, $p<0.05$).

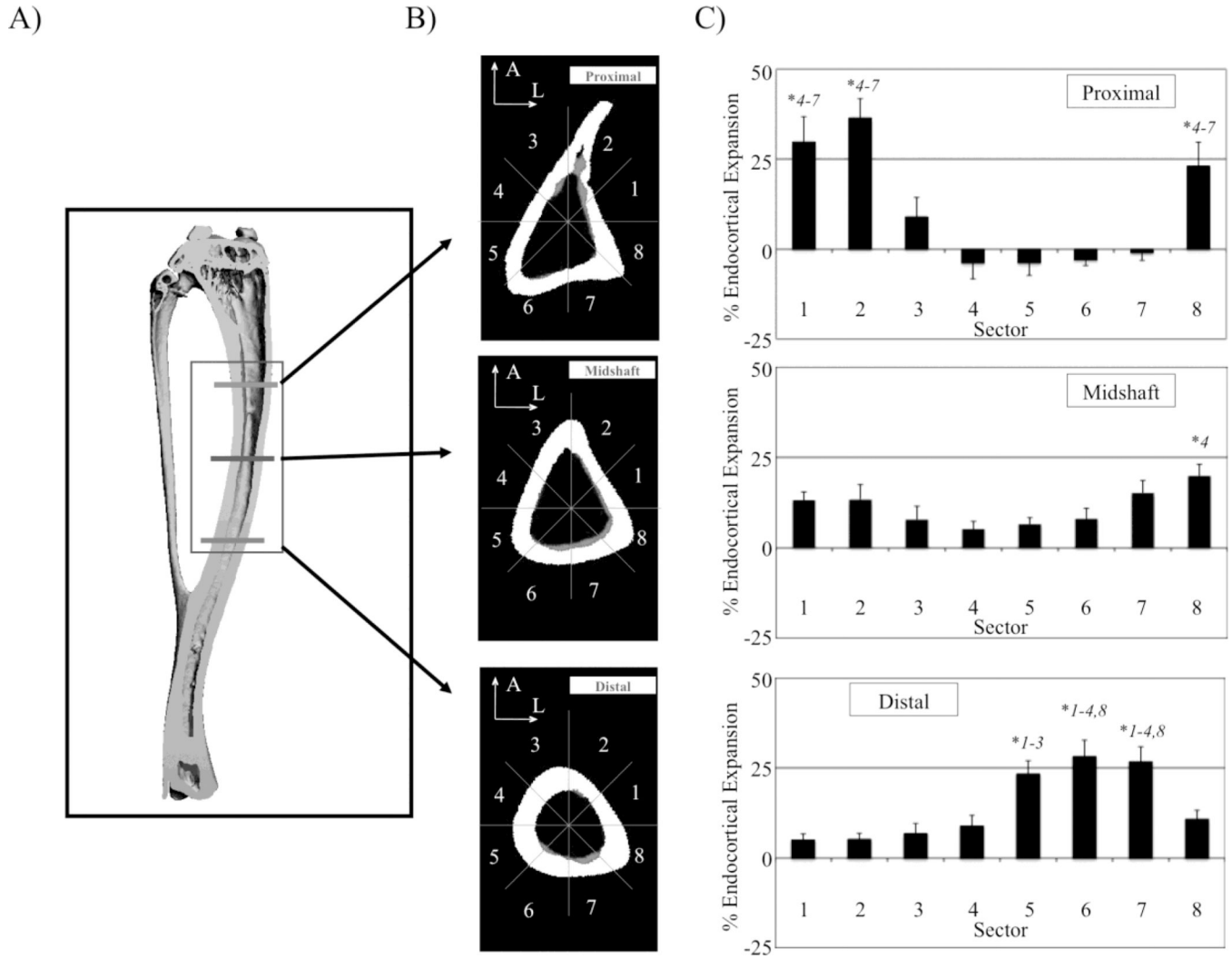

Fig. 4.

Bone loss investigated at three locations equally spaced and flanking the analyzed tibia diaphysis volume (A) showed focal patterns of endocortical expansions that differ along the long axis of the bone (B, bone resorption in gray). Bone loss in the proximal cross-section was greatest in the Anterior/Lateral surface (C- Proximal), while bone loss in the distal cross-section was greatest in the Posterior/Medial surface (C- Distal). Endocortical expansion at the tibia midshaft was the most uniform around the circumference of the bone cross-section, yet still varied significantly (C- Midshaft). Significant increases in endocortical expansion across sectors are denoted by an asterisk followed by the sector number(s) in which a significant difference was determined ($p<0.05$).

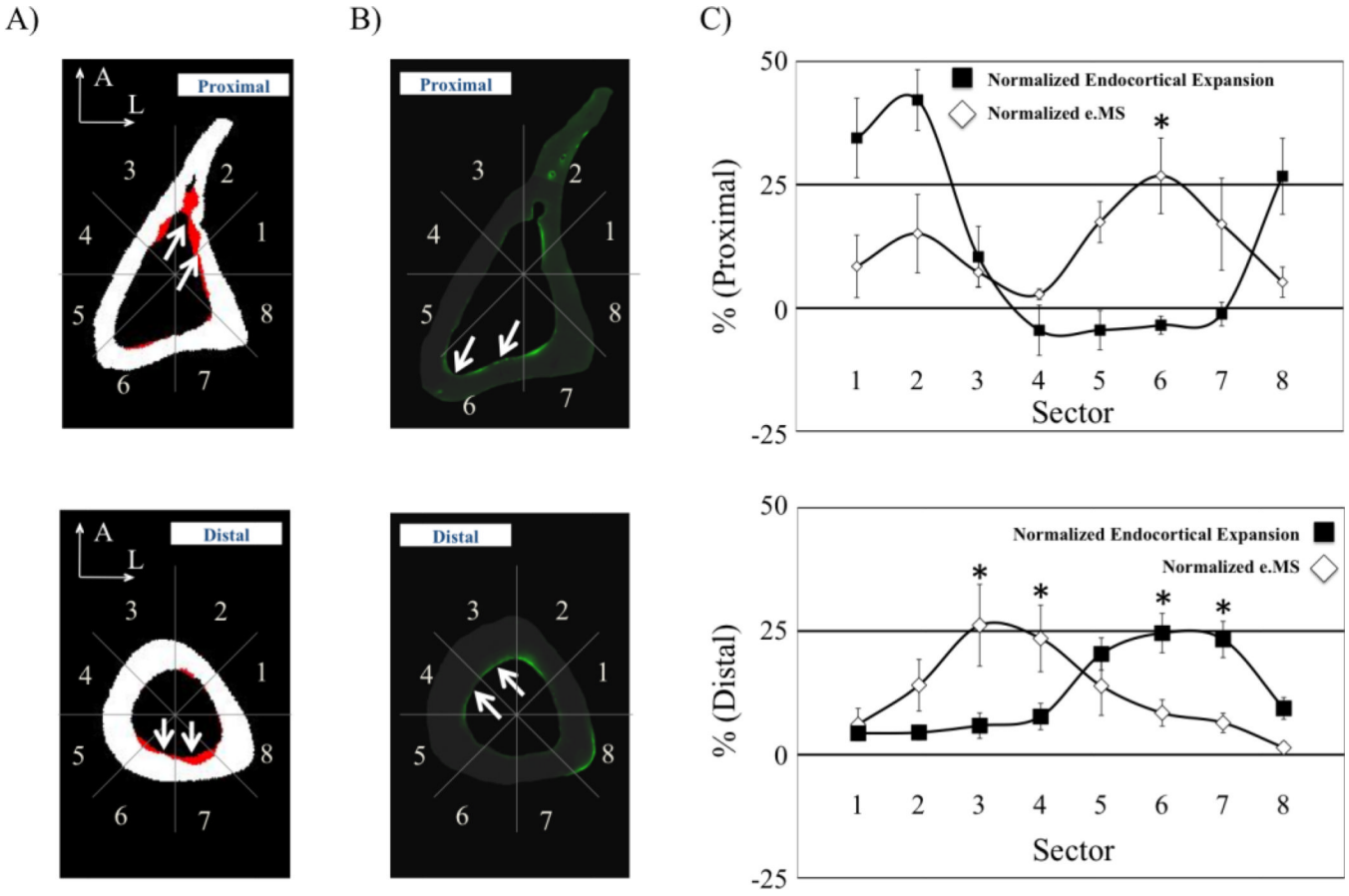

Fig. 5.

At the Proximal cross-section, osteoclast activity was greatest in the Anterior/Lateral cortex (A-Proximal, white arrows highlighting resorption in red), while the contribution of osteoblast activity was highest on the Posterior/Lateral surface (B-Proximal, white arrows highlighting Calcein labeling in green). Conversely, at the Distal cross-section, endocortical expansion occurred primarily in the Posterior cortex (A-Distal, white arrows) while osteoblast activity was greatest on the Anterior/Medial surface (B-Distal, white arrows). Sectors with significant differences between normalized endocortical expansion and normalized e.MS are noted (C; *, $p<0.05$).

Table 1

Mean Absolute Percent Error in Registered Versus Unregistered Validation Group [mean ± s.e.][a]

		Periosteal	Cortical	Endocortical
Whole Bone (n=6)	Registered	0.31 ± 0.08%	0.37 ± 0.10%	0.46 ± 0.15%
	Unregistered	0.33 ± 0.05%	0.36 ± 0.10%	0.41 ± 0.20%
Cross-Section (n=6[b])	Registered	0.36 ± 0.07%	0.60 ± 0.08%	0.89 ± 0.11%
	Unregistered	0.42 ± 0.05%	0.66 ± 0.07%	0.93 ± 0.20%
Site-Specific (n=6[b])	Registered	1.95 ± 0.27%*	1.94 ± 0.24%*	3.52 ± 0.31%*
	Unregistered	15.41 ± 3.77%	11.40 ± 2.92%	23.6 ± 5.66%

[a] Perfect spatial reproduction of the Day 0 scan would result in 0% mean absolute error.

[b] Individual animal means for all possible comparisons (Cross-Section: 300; Site-Specific: 1800) were used for this analysis.

* Significantly reduced vs Unregistered ($p<0.05$).

Table 2

e.MS Per Sector at Distal and Proximal Cross Sections [mean ± s.e.]

		Proximal	Distal
Sector	**1**	17.1 ± 12.8%	10.8 ± 5.8%
	2	30.5 ± 16.0%	24.9 ± 9.2%
	3	14.7 ± 6.0%	46.3 ± 14.6%
	4	5.7 ± 2.1%	41.6 ± 11.9%*
	5	35.2 ± 8.4%	24.6 ± 10.5%
	6	54.2 ± 15.5%*	14.9 ± 4.7%
	7	34.3 ± 18.8%	11.4 ± 3.5%
	8	10.6 ± 6.2%	2.5 ± 2.1%

*Significant difference between Proximal and Distal cross-sections ($p<0.05$)